José P. Suárez; Ángel Plaza; Tania Moreno
Geometric diagram for representing shape quality in mesh refinement

Persistent URL: http://dml.cz/dmlcz/702979

# GEOMETRIC DIAGRAM FOR REPRESENTING SHAPE QUALITY IN MESH REFINEMENT

José P. Suárez[1], Ángel Plaza[1,2] and Tania Moreno[3]

[1] MAGiC. Division of Mathematics, Graphics and Computation, IUMA, Information and Communication Systems, University of Las Palmas de Gran Canaria
Canary Islands, Spain
josepablo.suarez@ulpgc.es

[2] Department of Mathematics, University of Las Palmas de Gran Canaria
Canary Islands, Spain
angel.plaza@ulpgc.es

[3] Faculty of Mathematics and Informatics, University of Holguín, Avenida XX Aniversario, vía Guardalavaca, Holguín, Cuba
tmorenog@facinf.uho.edu.cu

**Abstract:** We review and discuss a method to normalize triangles by the longest-edge. A geometric diagram is described as a helpful tool for studying and interpreting the quality of triangle shapes during iterative mesh refinements. Modern CAE systems as those implementing the finite element method (FEM) require such tools for guiding the user about the quality of generated triangulations. In this paper we show that a similar method and corresponding geometric diagram in the three-dimensional case do not exist.

**Keywords:** mesh generation, longest-edge refinement, geometric diagram, mesh regularity

**MSC:** 65L50, 65M50

## 1. Introduction

Mesh generation and, in particular, the construction of 'quality' meshes is a major issue in many fields where computer modeling and engineering analysis are extensively used [4, 12]. Some mesh smoothing and mesh optimization strategies are described in [2, 3, 5, 6], and also different mesh quality metrics have been proposed in recent years [9].

For example in the finite element method (FEM), equilateral triangles are favored over obtuse or skinny triangles. Many of these methods employ forms of local and global triangle subdivision and seek to maintain well-shaped triangles. Here we consider several popular triangle subdivision schemes.

When refining a mesh, the aim is to use a given triangle subdivision scheme that may preserve the minimum angle condition in the sense that such smallest angle keeps as high as possible, [1, 15]. In the last years, many triangle partitions has been studied, including schemes using more than one point to configure the triangle halving [17]. The approach for partitioning single triangles is further used to develop algorithms that for a given input mesh and some refinement criteria through the elements, a new mesh is obtained with more element detail, see e.g. [8, 11].

Lastly the idea of using a two-dimensional diagram for representing triangle shape in mesh generation points to the works of [8, 13, 16]. While in [13] a more comprehensive development, theory and application of such diagram can be found, where the concept of normalization of triangles by the longest edge is the key for the computational construction of the diagram. It is worth to mention that this is not a novel idea. Already in 1939, Tuckey [18] observed the potential of using same normalization idea to construct a diagram in 2D. The main reason to introduce this diagram was the solution of triangles. In 1943 Tuckey presented a variation of the diagram for the same purpose, obviously a handle-method very far away of any computational automation. The idea behind the diagram is scaling any triangle so that the length of its longest edge is equal to one and the other sides $x$ and $y$ are in descending order; then the point with coordinates $x$ and $y$ will represent the triangle.

In this work we review some previous results on construction of a geometric diagram for assessing mesh quality, see [10, 13]. While diagram suits perfectly for the two-dimensional case its counterpart in the three-dimensional case does not. To demonstrate this, we provide a result showing that the normalization process of tetrahedra by the longest edges of tetrahedra is not possible, and thus the extension of a similar diagram to 3D case is not feasible either.

## 1.1. Mesh refinement schemes

By the longest-edge (LE) partition of a triangle $t_0$ we mean a subdivision scheme where the midpoint of the longest edge of a triangle $t_0$ is joint with the opposite vertex, see Figure 1 (a).

Another subdivision strategy of our interest is the 4TLE (Four Triangles Longest Edge) strategy [14], see Figure1(b). In this scheme, subdivision produces some subtriangles that are similar to certain previous triangles in the refinement tree generated. However, the other subtriangles are not in such similarity classes yet and we refer to them as new dissimilar triangles.

The other well-studied partition is the 7TLE (Seven Triangles Longest Edge) [10] where we position two equally spaced points per edge and, then the interior of the triangle is divided into seven sub-triangles in a manner compatible with the subdivision of the edges. Three of the new sub-triangles are similar to the original, two are similar to the new triangle also generated by the 4T-LE, and the other two triangles are, in general, better shaped [10].

It should be noted that, due to parallelism, the first three sub-triangles obtained are similar to the initial one $t_0$, whereas the second two sub-triangles are similar to
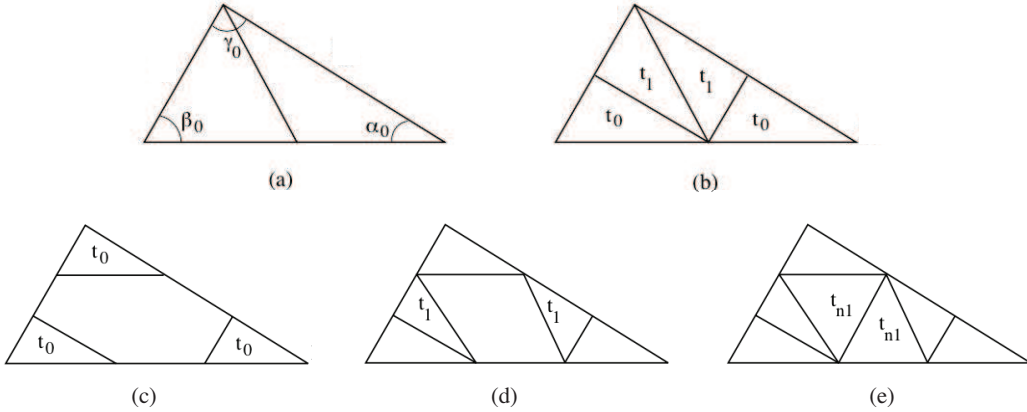
Figure 1: (a) LE (longest-edge) partition, (b) 4TLE (Four Triangles Longest Edge), (c)-(e) 7TLE (Seven Triangles Longest Edge).

the first-class Rivara triangle $t_1$. Finally, the last two triangles are not given with the 4T-LE partition and, consequently, will be called here, $t_{n1}$. Note also that the area of sub-triangles $t_0$ and $t_1$ is 1/9 of the area of the initial triangle, whereas the area of each sub-triangle $t_{n1}$ is 2/9 of the area of the initial triangle.

## 2. Geometric diagram

Now we present the main ideas for the construction of the geometric diagram in the context of 2D mesh refinement, for details, see [10, 13].

We first consider the normalized triangles which share the longest edge defined by the points $(0,0)$ and $(1,0)$. The apex of the triangle $(x, y)$ is a point chosen uniformly in the region defined by the unit circle centered at $(1,0)$, and by the vertical line $x = \frac{1}{2}$ (see Figure 2).

The geometric diagram is constructed as follows: (1) For a given triangle (or sub-triangle) the longest edge is scaled to have the unit length. This forms the base of the diagram. (2) It follows that the set of all triangles is bounded by this horizontal segment (longest edge) and by two bounding exterior circular arcs of unit radius, as shown in Figure 3.

In the diagram of Figure 3 (left) we demarcate shaded regions to classify triangles based on ranges of the *largest angle* $\gamma$ within circular arcs as shown; e.g. the lowermost subregion corresponds to obtuse triangles with large angles near $\pi$ and the uppermost subregion (exterior to the semicircle of radius $\frac{1}{2}$ centered on the unit base) corresponds to acute-angled triangles. The equilateral triangle corresponds to the apex with coordinates $\left(\frac{1}{2}, \frac{\sqrt{3}}{2}\right)$. As the vertex of a triangle moves from this point along either boundary arc, the maximum angle increases from $\frac{\pi}{3}$ to approach a right angle at the degenerate 'needle triangle' limit near $(0,0)$ or $(1,0)$. Similarly, in the
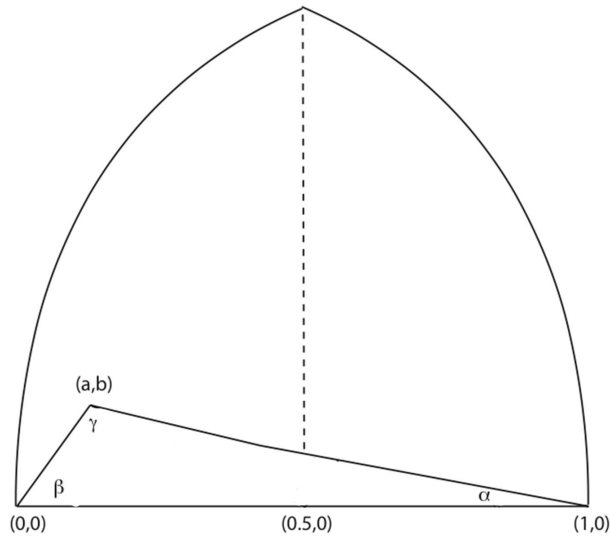
227

Figure 2: A random triangle normalized by its longest edge inside the diagram region.
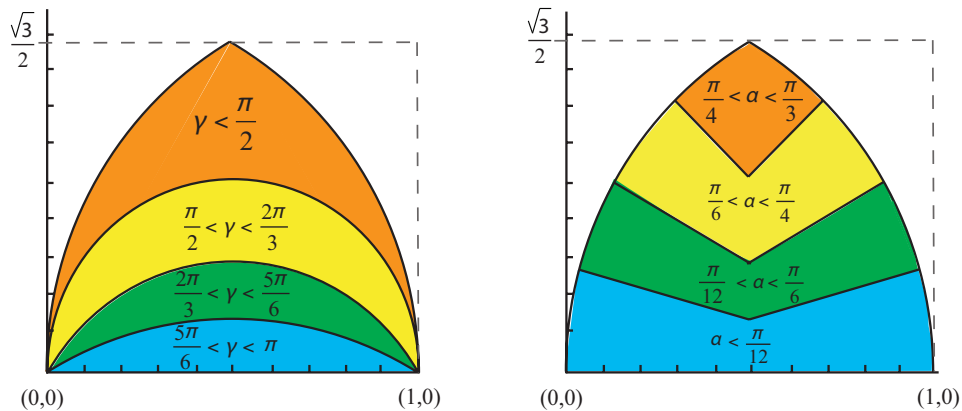


Figure 3: Diagram for triangles showing different regions corresponding to variations values of the largest angle $\gamma$ and the smallest angle $\alpha$.

diagram of Figure 3 (right) we demarcate by segments of straight lines emanating from $(0,0)$ and $(1,0)$, shaded subregions that bound the *smallest angle $\alpha$* of a triangle. Color shading makes the respectively subregions easier to identify. The topmost subregion between the exterior circular arcs and the lines for smallest angle $\alpha = \frac{\pi}{4}$ corresponds to triangles with $\frac{\pi}{4} < \alpha < \frac{\pi}{3}$. The v-shaped subregion below this is for the case $\frac{\pi}{6} < \alpha < \frac{\pi}{4}$ and so on, with the lowest shaded region for $\alpha < \frac{\pi}{12}$. From the shaded regions in these two diagrams, it is clear that slender triangles with large

obtuse angles and small acute angles will be located close to the center part of the base and triangles close to equilateral shape will be near the apex of the diagram. It follows that one can use this diagram to investigate the evolution of triangle shapes under subdivision as we show further.

It is obvious that the right triangle (i.e. $\gamma = \pi/2$) is a separator of the familiar acute and obtuse triangle classes. The locus of points corresponding to this separator is easily identified from elementary geometry as the semicircle with unit diagonal base in our mapping diagram. Points above this semicircle $\left|z - \frac{1}{2}\right| = \frac{1}{2}$, where $z = (x, y)$ is the apex of a triangle, correspond to acute triangles and points below correspond to obtuse triangles. We will not show this semicircle in the color class diagrams following, but this property should be kept in mind for other reasons. Further we focus on the number of dissimilar triangles that are generated by various triangle subdivision schemes.

## 2.1. Generating the diagram by the Monte-Carlo experiment

Once we have depicted the basics involved in the diagram, we focus on computing those regions that are specifically related to the shapes appearing in a given triangle partition, for example 4TLE, 7TLE, etc.

Let us begin by describing a Monte-Carlo computational experiment that can be used to visually distinguish the classes of triangles by the number of dissimilar triangles generated by the 4TLE partition. We proceed as follows: (**1**) Select a point within the mapping domain comprised by the horizontal segment and by the two bounding exterior circular arcs. This point $(x, y)$ defines the apex of a target triangle. (**2**) For this selected triangle, 4TLE refinement is successively applied as long as a new dissimilar triangle appears. This means that we recursively apply 4TLE and stop when the shapes of new generated triangles are the same as those already generated in previous refinement steps. (**3**) The number of such refinements to reach termination defines the number of dissimilar triangles associated with the initial triangle and this numerical value is assigned to the initial point $(x, y)$ chosen. (**4**) This process is progressively applied to a large sample of triangles (points) uniformly distributed over the mapping domain. (**5**) Finally, we graph the respective values of dissimilar triangles in a corresponding color map, see Figure 4 (left).

## 2.2. Structure of regions for the 4TLE refinement

For clarity, the number of dissimilar triangles has been added inside several colored regions in Figure 4. Thus, the numerical value 2 corresponds to two dissimilar triangles is associated with the region above the pair of arcs that intersect on the vertical line of symmetry near the point $(0.5, 0.3)$. The region below this corresponds to 3 dissimilar triangles, and so on as the base is approached. Viewed another way, obtuse needle-like triangles near the base will require many refinements before new dissimilar triangles no longer appear. Later, we will explore this point and plot associated trajectories corresponding to migration of new triangles.

From Figure 4 (right), we deduce that the separator for classes 2 and 3 in case
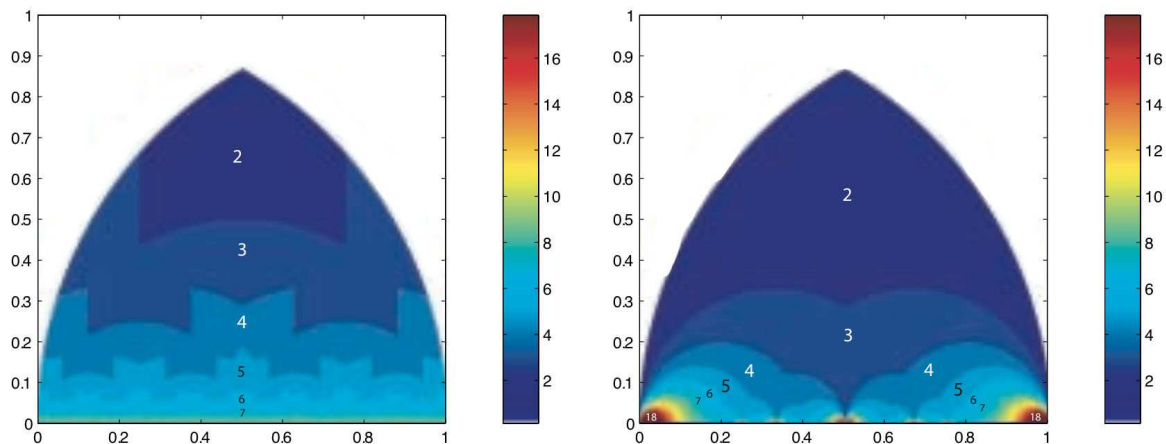
Figure 4: Subregions for dissimilar triangle classes generated by the Monte-Carlo simulation for the 4TLE (left) and the 7TLE (right) partitions, respectively.

of 7TLE is given by the segments of two circles of radius $\frac{1}{3}$ centered respectively at $x = \frac{1}{3}$ and $x = \frac{2}{3}$. That is, the curves $\left| z - \frac{1}{3} \right| = \frac{1}{3}$ and $\left| z - \frac{2}{3} \right| = \frac{1}{3}$. The curves for the subsequent separator between 3 and 4 have slightly more complicated shapes. Moreover, this shape is again evident on two smaller scales at the level of the next separator between 4 and 5. The pattern appears to continue to repeat in a fractal-like manner as the higher value separators are identified. A more formal mathematical approach, based on mapping in the complex plane, follows and utilizes the concept of antecedent triangle for the 4TLE partition.

One may use two functions, named $f_L$ and $f_R$ showing a 'trace back' from the equilateral triangle $t_0$, with apex $\left( \frac{1}{2}, \frac{\sqrt{3}}{2} \right)$, see Figure 5 (a). From equilateral triangle $t_0$ situated on the intersection of the exterior boundary curves, the only antecedent that generates it after subdivision is triangle $t_1$. Note that $t_1$ is an obtuse triangle located exactly where the pair of boundary curves intersect on the vertical line of symmetry at the point $y = \frac{\sqrt{3}}{6}$. Continuing the traceback, this obtuse triangle $t_1$ is the result of the subdivision of two antecedent triangles as marked, with the right antecedent denoted $t_2$ and the left one being symmetrically located in the left part of the diagram as expected. Again, each of these $t_2$ triangles is located at the intersection of two boundary curves. The next pair of antecedents of the right half from left to right are $t_3'$ and $t_3$ respectively. As before, $t_3'$ and $t_3$ are located at the intersections of respective pairs of boundary curves that demarcate a change in similarity class and the process continues downward in the diagram with the antecedents approaching the degenerate case of planar obtuse triangles on the horizontal line. Another traceback example is given in Figure 5 (b), starting with apex $(0.67, 0.43)$ (and obviously has a similar path reflected in $x = \frac{1}{2}$).

The class separators determined experimentally by the Monte-Carlo experiment may also be generated mathematically as a recursive composition of left and right
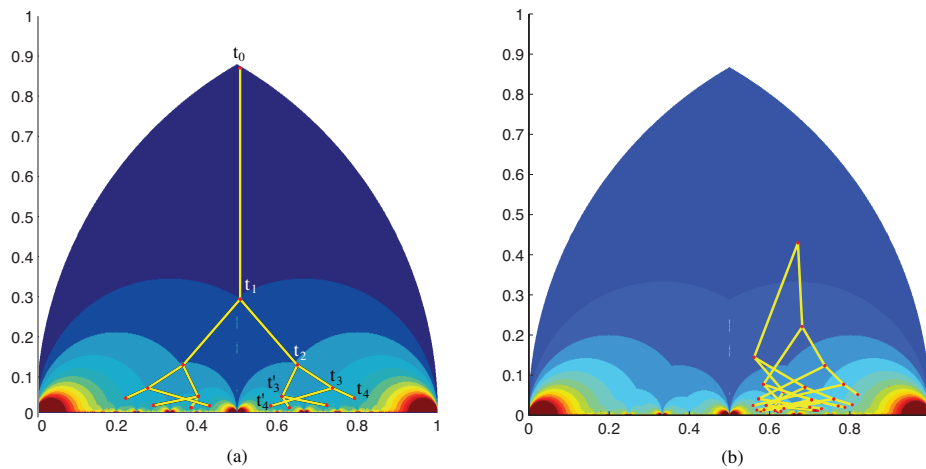
Figure 5: Traceback curves showing antecedents in successive regions: (a) traceback from equilateral triangle apex with antecedents on border curves and (b) traceback from acute triangles interior to region.
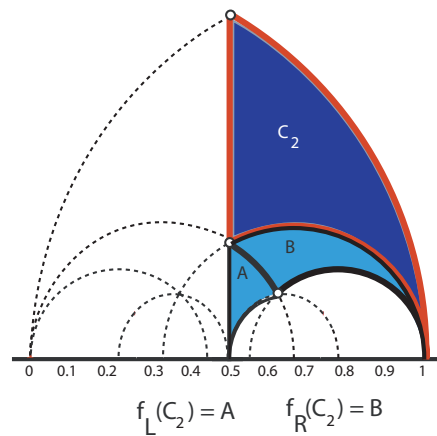


Figure 6: Boundary curves for the separator of order 2 and 3 in the 4TLE partition.

maps $f_L$ and $f_R$, for details see [13]. Then it follows that a set of boundary curves for those separators is easily obtained, see Figure 6.

## 2.3. Structure of regions for the 7TLE refinement

We recursively apply 7T-LE and stop when the shapes of new generated triangles are the same as those already generated in previous refinement steps. The number of such refinements to reach termination defines the number of dissimilar triangles associated with the initial triangles associated with the initial triangle and this numerical value is as- signed to the initial point $(x, y)$ chosen. This process is

progressively applied to a large sample of triangles (points) uniformly distributed over the domain. Finally, we graph the respective values of dissimilar triangles in a corresponding color map to obtain the result in Figure 4 (right).

Note that for the 7TLE partition, a lower bound for the maximum of the smallest angles for triangles $t_n 1$ is $\alpha = 30°$ corresponding to the apex with $x = 1$, or the apex with $x = 3$.

Unfortunately, deriving classes separator as done respectively for the 4TLE is still an open problem. The main reason is that the 7TLE refinement produces seven new triangles that complicates the calculation of functions $f_L$ and $f_R$.

Note that the diagram is useful to tackle the so-called self-improvement property of partitions for 4TLE, 7TLE and others triangle schemes. It also is feasible to use the diagram for assessing which algorithm is more convenient for mesh refinement. For example, using combinations of partitions, i.e. using one type for some targeted triangle cases and the other type for the others may yield improved algorithms. For example, in [10] it has been proposed a combined scheme for improvement of the mesh, by combining longest-edge based with other self-similar partitions, depending on the number of points inserted per edge.

## 3. Toward a geometric diagram in the three-dimensional space

Concerning extension of the previous geometric diagram to the three-dimensional case, we give some helpful ideas resulting to a negative conclusion: there does not exist a similar geometric diagram for representing mesh quality during mesh refinements in 3D.

We say that two triangles (two tetrahedra in three dimensions) are in the same similarity class if there exists a similarity transformation that transforms one of these triangles (tetrahedra in three dimensions) into the other.

**Theorem 1.** *Let us have a given segment $\overline{AB}$ of length $1$ in the Euclidean plane. Let $\mathcal{T}$ be the class of all triangles $T$ such that $\overline{AB}$ is the longest edge of $T$. Then there exists a subclass $\mathcal{D}$ of $\mathcal{T}$ satisfying the following conditions.*

1. *For each similarity class of triangles $\mathcal{S}$, there are one and only one element of $\mathcal{S}$ in $\mathcal{D}$.*

2.

$$diam(\bigcup_{T \in \mathcal{D}} T) = 1$$

As a consequence of Theorem 1 we have that for the two-dimensional case, there exists a diagram for normalizing triangles with respect to the longest edge, as showed in Section 2. The utility of this diagram lead us to think about the possibility of make an analogous diagram for the representation of tetrahedra in the three-dimensional Euclidean space. However, we will see some difficulties that appears in the attempt to construct a natural generalization of this diagram in the three-dimensional case.

**Theorem 2.** *Let us have a given segment $\overline{AB}$ of length $1$ in the three-dimensional Eucidean space. Let $\mathcal{D}$ be the geometric place of all tetrahedra $\mathcal{T}$ such that $\overline{AB}$ is one longest edge of $\mathcal{T}$. Then it follows that the diameter (maximum of longest edge) in the set $\mathcal{D}$ is greater than $1$.*

**Skecth of the Proof:** Note that $\mathcal{D}$ include a regular tetrahedron $ABP_1P_2$ and a tetrahedron $ABQ_1Q_2$ such that $|\overline{Q_1A}| = |\overline{Q_1B}| = |\overline{Q_2A}| = |\overline{Q_2B}| = \frac{\sqrt{2}}{2}$ and the dihedral angle between faces $ABQ_1$ y $ABQ_2$ equals $150°$. We will see that there exist $i_0$, $j_0$, $i_0 \in \{1, 2\}$, $j_0 \in \{1, 2\}$ such that $|\overline{P_{i_0}Q_{j_0}}| > 1$.

Let $M$ be the midpoint of $\overline{AB}$. Note that $\angle P_1MP_2 = \arccos(\frac{1}{3}) = 70.5288°$, $\angle Q_1MQ_2 = 150°$ and the points $M$, $P_1$, $P_2$, $Q_1$, $Q_2$ are coplanar. Then there exist $i_0$, $j_0$, $i_0 \in \{1, 2\}$, $j_0 \in \{1, 2\}$ such that $\triangle P_{i_0}MQ_{j_0}$ is an obtuse triangle in $M$.

Moreover, $|\overline{P_iM}| = \frac{\sqrt{3}}{2}$, $i \in \{1, 2\}$ and $|\overline{Q_jM}| = \frac{1}{2}$, $j \in \{1, 2\}$ from where in the obtuse triangle $\triangle P_{i_0}MQ_{j_0}$ we have

$$|\overline{P_{i_0}Q_{j_0}}| > \sqrt{|\overline{P_{i_0}M}|^2 + |\overline{Q_{j_0}M}|^2} = \frac{3}{4} + \frac{1}{4} = 1.$$

We then conclude that

$$\mathrm{diam}(\bigcup_{T \in \mathcal{D}} T) > 1$$

$\square$

## 4. Conclusions

In this work we have recovered the idea of the geometric diagram for assessing quality in triangle mesh refinement. In FEM, error indicators give the trends of the behavior of the solution through an iterative process. Classically, the angle condition has been set as the standard form for the good quality of a mesh, where acute, right, and in general, those triangle shapes very close the regular triangles behave better, [15, 1]. In this work we provide a visual tool, called the geometric diagram, for inspecting shape evolution in the refinement of meshes. Fortunately, the tool is clearly of utility as has been shown in the study of two triangle partition schemes, 4TLE and 7TLE. In addition, we provide a new result consisting in confirming that an extension to a similar geometric diagram for the three-dimensional case is not possible, partially due to the impossibility to normalize by the longest edge of tetrahedra. This last result however, open to a new scene where an idea of different geometric diagram by normalizing e.g. edges or faces of tetrahedra may be feasible.

## References

[1] Babuška, I. and Aziz, A. K.: On the angle condition in the finite element method. SIAM J. Numer. Anal. **13** (1976), 214–226.

[2] Branets, L. and Carey, G. F.: Smoothing and adaptive redistribution for grids with irregular valence and hanging nodes. In: *Proceedings of the 13th International Meshing Roundtable*, pp. 333–344, 2004.

[3] Branets, L. and Carey, G. F.: A local cell quality metric and variational grid smoothing algorithm. Engrg. Comput. **21** (2005), 19–28.

[4] Carey, G. F.: *Computational grids: generation, refinement and solution strategies*. Taylor and Francis, 1997.

[5] Freitag, L. A. and Plassman, P.: Local optimization-based simplicial mesh untangling and improvement. Int. J. Num. Meth. Engrg. **49** (2000), 109–125.

[6] Garimella, R. V., Shashkov, M. J., and Knupp, P. M.: Triangular and quadrilateral surface mesh quality optimization using local parametrization. Comp. Meth. Appl. Mech. and Engrg. **193** (2004), 913–928.

[7] Hannukainen, A., Korotov, S., and Křížek, M.: On numerical regularity of the face-to-face longest-edge bisection algorithm for tetrahedral partitions. Sci. Comput. Program. **90** (2014), 34–41.

[8] Hannukainen, A., Korotov, S., and Křížek, M.: On global and local mesh refinements by a generalized conforming bisection algorithm. J. Comput. Appl. Math. **235** (2010), 419–436.

[9] Knupp, P. M.: Algebraic mesh quality metrics. SIAM J. Sci. Comput. **23** (2001), 193–218.

[10] Márquez, A., Moreno-González, A., Plaza, Á., and Suárez, J. P.: The seven-triangle longest-side partition of triangles and mesh quality improvement. Finite Elem. Anal. Des. **44** (2008), 748–758.

[11] Padrón, M. A., Suárez, J. P., and Plaza, A.: Refinement based on longest-edge and self-similar four-triangle partitions. Math. Comput. Simulation **75** (2007), 251–262.

[12] Knupp, P. M. and Steinberg S.: *The fundamentals of grid generation*. CRC Press, Boca Raton, FL, 1994.

[13] Plaza, Á., Suárez, J. P., and Carey, G. F.: A geometric diagram and hybrid scheme for triangle subdivision. Comput. Aided Geom. Des., **24** (2007), 19–27.

[14] Plaza, Á., Suárez, J. P., Padrón, M. A., Falcón, S., and Amieiro, D.: Mesh quality improvement and other properties in the four-triangles longest-edge partition. Comput. Aided Geom. Design **21** (2004), 353–369.

[15] Korotov, S., Křížek, M., and Kropáč, A.: Strong regularity of a family of face-to-face partitions generated by the longest-edge bisection algorithm. Comput. Math. Math. Phys. **48** (2008), 1687–1698.

[16] Rivara, M. C.: LEPP-bisection algorithms, applications and mathematical properties. Appl. Num. Math. **59** (2009), 2218–2235.

[17] Suárez, J. P., Moreno, T., Abad, P., and Plaza, Á.: Properties of the longest-edge $n$-section refinement scheme for triangular meshes. Appl. Math. Letters **25** (2012), 2037–2039.

[18] Tuckey, C. O.: A diagram for the study and solution of triangles. The Mathematical Gazette, **23** (1939), 150–154.

[19] Tuckey. C. O.: A diagram for the solution of triangles. The Mathematical Gazette, **27** (1943), 1–3.